Real-time Through-wall Imaging Using an Ultrawideband Multiple-Input Multiple-Output (MIMO) Phased Array Radar System*

Tyler S. Ralston, Gregory L. Charvat,
and John E. Peabody
MIT Lincoln Laboratory
244 Wood Street, Lexington, MA 02420-9185
Email: tralston@ll.mit.edu, gregory.charvat@ll.mit.edu,
and jpeabody@ll.mit.edu

Abstract—A real-time acquisition and processing architecture has been developed for an ultrawideband (UWB) S-band (2-4 GHz) multiple-input multiple-output (MIMO) phased array radar system that facilitates greater than 10 Hz imaging rates, providing a video-like radar image of what is behind a concrete wall. Video rate imaging enhances the interpretability of range vs. range through-wall and free-space radar imagery. Images are formed without a-priori information. Video frame-rate imaging is achieved by designing an electronically switched bi-static array using high-performance microwave components, a multi-threaded data pipeline, and efficient hardware-accelerated processing algorithms. Experiments successfully image low radar cross section (RCS) objects, fast moving objects in free-space, and a human behind a 10 cm-thick solid concrete wall.

I. Introduction

The ability to geolocate moving targets through a solid wall would improve situational awareness on the urban battlefield. In this paper a radar sensor that provides real-time video frame-rate imaging through a concrete wall is shown. Video frame-rate imaging is essential for intuitive human interpretation of radar imagery, where situational awareness is gained by the operator watching objects moving on the opposite side of an opaque wall.

Some existing human-portable through-wall radar sensors require the user to place the radar unit directly on (or close to) the wall resulting in limited stand-off range performance ([1], [2] and [3]). A more complicated system requires three individual data sets to be acquired by manually repositioning an antenna array to synthesize a larger aperture [4], therefore, this solution does not provide real-time surveillance. A larger 2 m long 4 element phased array was demonstrated [5], but it potentially suffers from false detections due to ghosting effects as evidenced in its imaging algorithm and sparse aperture. A switched antenna array using a UWB impulse transmitter and receiver provides a 3 Hz image rate [6], but requires a larger peak transmit power and a wider bandwidth data acquisition system compared to that of an

equivalent linear frequency modulated (LFM) radar sensor, thus increasing system cost and complexity. A full aperture with $\lambda/2$ spacing is implemented on a linear rail system and is capable of forming images with a synthetic aperture radar (SAR) algorithm ([7], [8]). This FMCW radar system is capable of operating at stand-off ranges by providing a relatively high average transmit power of 2 mW, but low peak-power of 10 mW, using long-duration (2.5-10 ms) LFM transmit pulses and a short-duration range gate implemented through use of high-circuit-Q analog IF filters. This rail SAR proves to be effective at imaging through a 10 cm-thick concrete wall at a stand-off range of 9.1 m, where stand-off range is advantageous for safety and covertness. Unfortunately, it requires approximately 20 minutes to acquire data, which is too slow for most practical through-wall applications. For this reason, a high-speed switched-antenna array implementation of this through-wall SAR has been developed ([7], [9]), where the time to acquire a full through-wall data set is reduced from 20 minutes to 1.9 seconds. This system is effective at imaging low RCS targets through a 10 cm-solid concrete wall but the 0.5 Hz imaging speed does not provide the needed continuous surveillance. While the time-division multiplexed (TDM) MIMO array architecture is sufficient to provide higher imaging rates, the processing throughput proves to be a bottleneck. The through-wall radar solution shown in this paper builds on the work above by increasing the image rate from 0.5 Hz to over 10 Hz by utilizing a high-speed SAR imaging architecture originally developed for real-time interferometric synthetic aperture microscopy [10]. This is supported by high-performance microwave components, a commercial-off-the-shelf (COTS) analog-to-digital converter (ADC) (1.25 MSPS at 16 bits), and a personal computer (PC).

To achieve video frame-rate radar imaging it is necessary to implement a pipelined data throughput and streamlined processing algorithm to interface to the radar system. In this paper the TDM MIMO radar design is discussed in Section

II, the data acquisition pipeline is described in Section III, and the real-time imaging algorithm is presented in Section IV. Estimated results are discussed in Section V. Experiments were conducted in free-space and through a 10 cm-thick solid concrete wall, these are described in Section VI. Future applications may require range-range-doppler processing which would require more computational overhead, for this reason a prototype imaging algorithm using a graphics processor unit (GPU) was implemented, results from preliminary benchmarks are shown in Section VII. Summary and future work are discussed in Section VIII.

II. RADAR IMPLEMENTATION

The block diagram is shown in Fig. 1. The core of this system is a range-gated FMCW radar device that transmits LFM chirps from 2-4 GHz in 1 ms with 2 W peak transmit power at 50 % duty cycle. This radar architecture is based on [8], where a range gate is implemented by the use of high-Q intermediate frequency (IF) filter FL1. This filter band-limits the decorrelated LFM prior to pulse compression resulting in an effective range-gate of the target by rejecting scattered returns from the air-wall boundary. This design provides maximum dynamic range and sensitivity for imaging targets behind a wall.

The transmit port of this FMCW radar is connected to a fan-out switch matrix made up of SW1-3, where the transmit port is fed to only one antenna element (ANT9-21) at a time. Similarly, the receive port of the radar system is connected to an 8-port switch (SW4) that connects to one LNA (LNA1-8) at a time. Each LNA is connected to and physically mounted to a receiver element (ANT1-8) to preserve the noise figure through feed line and system losses.

The antenna element (top layer shown in Fig. 2) is based on a combination of a Vivaldi and linear-tapered slot design and is capable of supporting at least 2-4 GHz of bandwidth with efficient radiation and useful E and H plane beamwidths.

The radar uses only a subset of all possible antenna combinations to form images which consist of 44 bi-static antenna element combinations whose effective phase centers approximate a linear array evenly spaced $\lambda/2$ [9]. These bi-static antenna combinations are shown in Fig. 3, where the large circles represent ANT1-21, the lines represent the bi-static combinations, and the small circles represent the effective phase centers.

All antenna switches (SW1-4) are solid state and digitally controlled by the PC. The TDM MIMO radar system sequences through each of the 44 bi-static combinations, acquiring one range profile at each. The PC controls the switches, pulses the transmitter, and digitizes the video (details in Section III). These tasks are executed in a continuous loop while simultaneously computing a SAR image and displaying it at a rate of 10.8 Hz (details in Section IV).

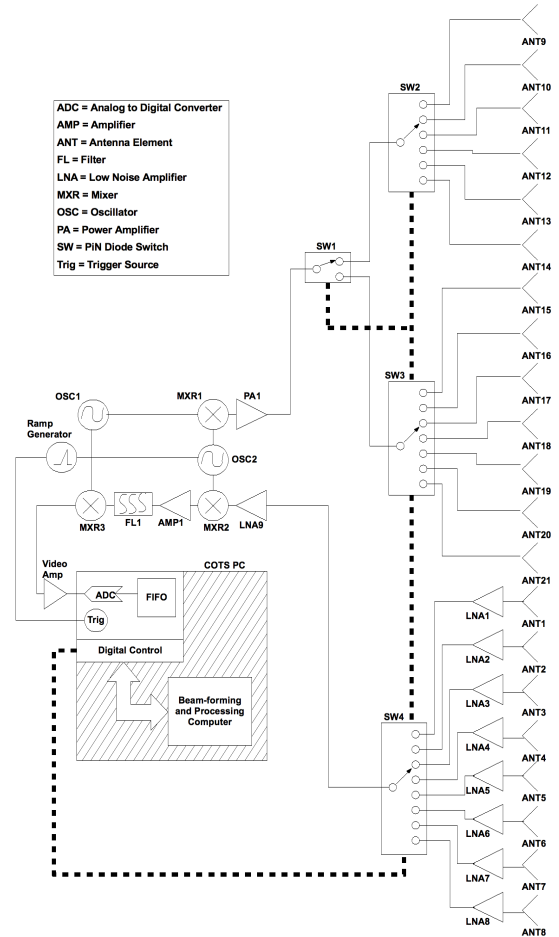A photograph of the complete radar system is shown in Fig. 4.

Fig. 1. Radar block diagram showing range-gated FMCW system connected to receive and transmit fan-out switch matrices which feed all antenna array elements.
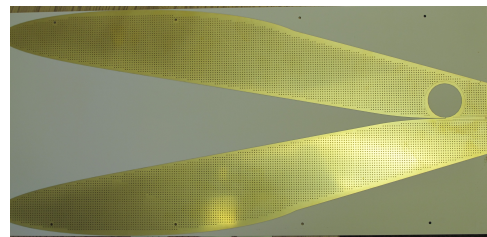

Fig. 2. Vivaldi and linear slot hybrid antenna element.

III. DATA ACQUISITION PIPELINE

The data acquisition (DAQ) system is composed of a multi-threaded software application developed using the Python scripting language executing on a PC and a National Instruments (NI) DAQ card (PCI-Express M-Series PCIe-6251). A block diagram of the DAQ system is shown in Figure 5. The DAQ system acquires data from the MIMO radar (Section III-A), provides system control through a graphical user in-
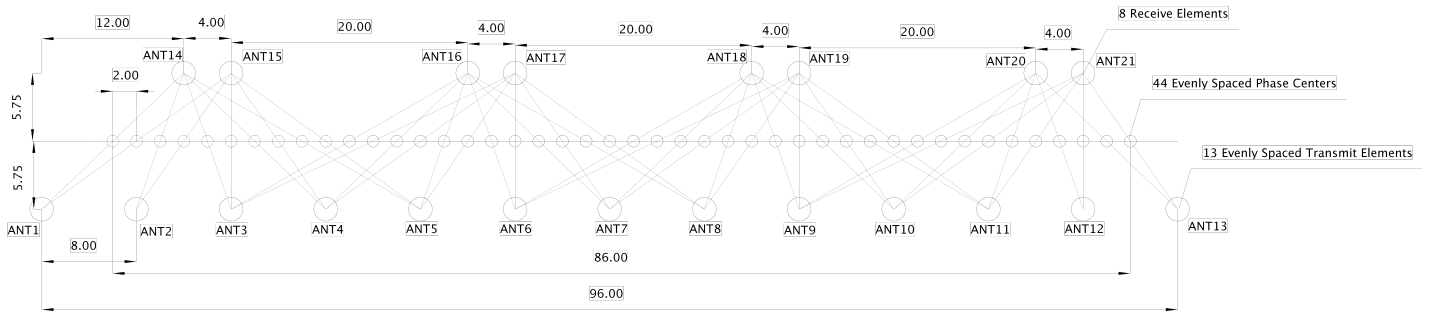
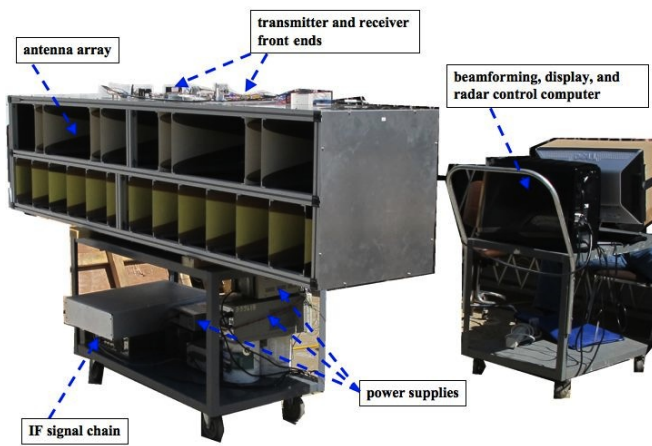Fig. 3. The TDM MIMO array layout (units in inches), antenna combinations, and phase center locations.

Fig. 4. TDM MIMO radar system.

Fig. 5. DAQ system block diagram.

terface (GUI) that displays the processed data (Section III-B), and establishes a pipeline to and from the data processing algorithms (Section III-C).

A. Data Acquisition

The NI DAQ card acquires data from the MIMO radar by leveraging a 250 MB/s bandwidth provided by the PCI Express bus inside of the PC. Four independent time-aligned NI tasks ensure proper triggering and sequenced data acquisition (Fig. 5). These tasks include a common trigger, the sample clock generator (SCG), analog output, and ADC.

A common trigger maintains time alignment between the data acquisition and the transmit pulse. For this alignment, the sample clock generator (SCG) task is triggered simultaneously with the ramp generator (which modulates OSC2 thereby producing the 2-4 GHz LFM transmit chirp). The analog output task generates a 1 KHz, 50% duty, square wave providing a rising edge that synchronizes the radar system.

The SCG task consists of two 32-bit counters configured to generate a gated finite pulse train at 1.25 MHz. Upon receiving the rising edge of the analog output task, the finite pulse train is generated. By gating the c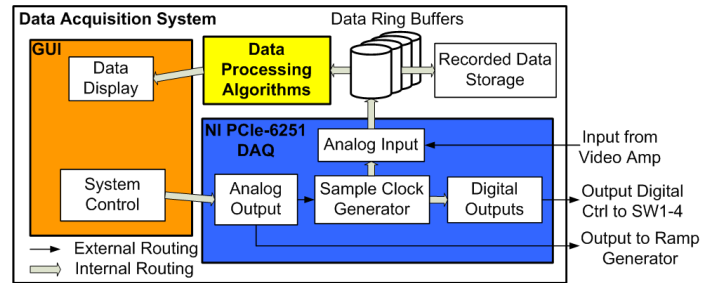ontinuous finite pulse train, the ADC operates in continuous mode, while only acquiring samples during the 1.2 msec acquisition period.

The acquisition window is adjustable to account for analog circuit delays within the radar system. This parameter ensures that the acquisition and the LFM chirp are aligned. This parameter is also used to configure the number of samples acquired within the analog input task.

A single-ended 16-bit resolution analog input channel is used to acquire the data from the radar. Configured to acquire 1500 samples at a clock rate of 1.25 MHz, this ADC task executes in continuous mode. The input from the SCG task controls the sample acquisition. ADC samples are acquired and stored within a first in first out (FIFO) buffer, internal to the NI DAQ during the period in which the SCG is generating a sample clock for the ADC task. Once the acquisition period completes, the FIFO data is moved into the data ring buffers in the PC memory using Direct Memory Access (DMA).

The digital output task controls the antenna switches SW1-4 and runs on the NI DAQ card. A FIFO buffer is programmed with the bi-static antenna combinations as described in Section III-B. Triggered by the falling edge of the SCG gating signal, this task outputs the next digital values within the FIFO buffer. The bi-static antenna selection is time aligned with the end of the data acquisition period.

B. Graphical User Interface (GUI)

The GUI controls the radar system and displays radar imagery in real-time (Fig. 6). The wxPython module provides Python bindings to the wxWindows framework and basic
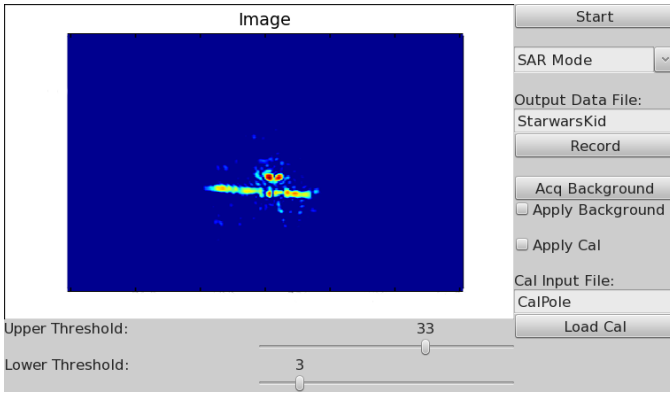
Fig. 6. Graphical User Interface with controls for starting the radar, imaging mode, output file name, record (on or off), record background, apply background, apply calibration, calibration input file name, load calibration, and dynamic range vernier sliders for both upper and lower threshold.

GUI objects used for constructing the overall layout including frames, buttons, and text fields enabling real-time system control. To increase the plotting capabilities within wxPython, Matplotlib (a 2D Python plotting library with integrated blit functions and block memory copy functions) is utilized to facilitate a greater than 10 Hz image rate.

The GUI provides two sliders located below the data image that control the upper and lower threshold of the dynamic range represented within the image. The widgets (buttons, selectors, sliders, etc.) on the right column of the GUI control the additional system functions.

C. Data Pipeline Interface

An interface is established between the Python-based DAQ system and the C++ imaging algorithms by wrapping them into a Python interface library using the Simplified Wrapper and Interface Generator (SWIG). To ensure proper data transfer between Python and C++, SWIG leverages a NumPy interface file that properly wraps NumPy arrays into C++ arrays. The DAQ system creates the NumPy array data ring buffers where the C++ data processing algorithms access the allocated memory structures for reading and writing. Overhead memory copy routines are avoided because both Python and C++ access the same memory by address.

IV. REAL-TIME BEAMFORMING ALGORITHM (RTBA)

This radar resolves targets using the range migration algorithm (RMA) [11], which is a near-field SAR imaging algorithm. Processing a single image with the RMA is computationally expensive. A careful implementation of the RMA was developed so that values are pre-computed and pre-organized in the memory whenever possible. A real-time beamforming algorithm (RTBA) in a C++ class was designed to execute a high-speed hardware optimized RMA. A Matlab executable (MEX) interface was designed to prototype the algorithm in a debug environment. This interface allows for continued development of processing routines.
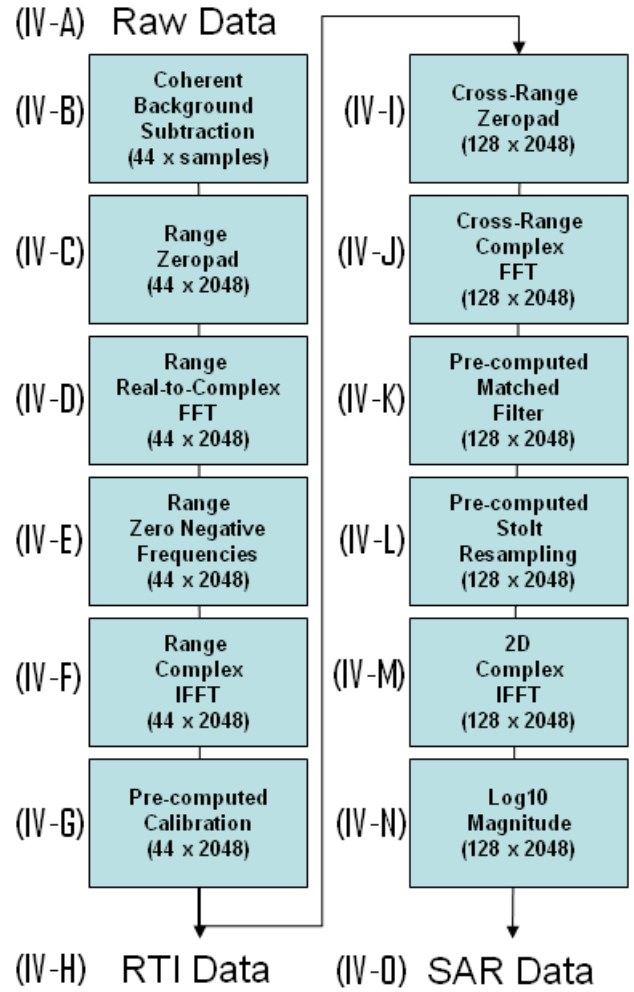

Fig. 7. RTBA block diagram (descriptions of each block discussed in Sections IV-A - IV-O).

Three imaging modes are supported by the RTBA and displayed by the GUI: raw real data, range time intensity (RTI), and synthetic aperture radar (SAR). Raw data and RTI are used for debugging purposes. SAR is the imaging mode and final product that the end user views when operating the radar.

Figure 7 shows the RTBA block diagram, where the output point for each mode is shown. The details of the pipeline are discussed in Sections IV-A - IV-O. The combination of these streamlined processes provides real-time imaging at a rate of 10.8 Hz.

A. Raw Data Input

Raw data is provided by the data acquisition pipeline from Section III as real valued 16-bit binary integers in a 44 column (the 44 TDM MIMO antenna element combinations) by 1500 rows (the 1500 ADC samples) matrix. The RTBA accepts data of any number of samples because the number of samples may vary in size to accommodate future changes in transmit bandwidth or analog circuitry settling times.

B. Coherent Background Subtraction

Two methods of coherent change detection are provided, coherent background subtraction and frame-to-frame change detection.

When using coherent background subtraction, raw data of the target scene is recorded and stored. The radar subtracts each new data set from the stored one displaying a coherent background subtracted image to the user thereby removing the source spectrum effects such as DC offset as well as non-moving background clutter. This method provides a coherent change detection mode where the target scene is subtracted from the original data set, showing all minute changes in the scene.

When using frame-to-frame change detection the radar subtracts the previous raw data set from the current one then displays the image of the difference. This provides a real-time moving target display, which shows anything that changes (or moves) between frames and removes static radar clutter from the displayed image of the target scene. The subtracted frame may be taken from several frames in the past, which provides detection of slowly moving targets.

C. Range Zero Pad

The output of the coherent background subtraction is zero-padded in the range dimension to the nearest power of 2 to ensure an optimized radix calculation of the fast Fourier transform (FFT). The Fastest Fourier Transform in the West (FFTW) is a hardware accelerated library that is used for all FFTs in the RTBA and helps to ensure maximum throughput.

D. Range Real-to-Complex FFT

Real data is converted to its complex analytic form by performing the Hilbert transform on the range spectra. The Hilbert transform is calculated by performing an FFT, making negative frequencies zero, and performing an inverse FFT (IFFT). The Fourier transform of a the real data is conjugate symmetric, therefore a real-to-complex FFT computes this efficiently.

E. Range Zero Negative Frequencies

The negative frequencies of the resulting range real-to-complex FFT are set to zero.

F. Range Complex IFFT

Complex IFFT is performed in the range domain.

G. Pre-Computed Calibration

The calibration matrix provides compensation for beam dependent delays as well as source dependent non-linearities resulting from analog waveform generator drift, temperature drift of microwave components, and array structure. The calibration matrix is computed from data acquired with a vertical copper pole that is approximately 1.5 m in height and 2.54 cm in diameter. The pole is placed in the center of the array at a specified distance of approximately 3 m. A calibration matrix is pre-computed by calculating the theoretic point target

response, dividing by the measured complex response, and regularizing. This pre-computed calibration matrix is then multiplied with the Hilbert transformed data.

H. RTI Data Output

After the pre-computed calibration is applied, the RTI data can be displayed by the GUI for debugging purposes.

I. Cross-Range Zero Pad

The calibrated data is symmetrically zero-padded to a power of 2 in the cross-range dimension (across the 44 columns).

J. Cross-Range Complex FFT

A complex FFT of the cross-range zero-padded columns is computed.

K. Pre-Computed Matched Filter

The matched filter moves the scene origin to the phase center. The matched filter matrix is pre-computed upon initialization and applied to the cross-range complex FFT data. To reduce computational cost further, if apodization is desired, the matched filter matrix is pre-computed with a weighting.

L. Pre-Computed Stolt Transform

The Stolt transform is a resampling of the 2D Fourier space along equal time-space contours. To minimize computational time, the linear spline resampling tables are pre-computed upon initialization. The Stolt transform is performed after the matched filter is applied.

M. 2D Complex IFFT

The 2D IFFT of the Stolt transformed data is computed to return to range and cross-range dimensions (image domain).

N. Log10 Magnitude

This radar system displays the relative logarithmic power of the scattered radar returns from the target scene. For this reason the base-ten logarithm of the magnitude squared voltage converts all pixels in the SAR image to dB relative power.

O. SAR Data Output

The SAR image is displayed by the GUI in real-time at a rate of 10.8 Hz. Each SAR image is computed while, at the same time, the data acquisition pipeline is controlling the radar and acquiring new data. All sub-systems working in concert provide real-time radar imagery at video frame-rates.

V. ESTIMATED RESULTS

A thermal-noise limited maximum range model was developed using the radar range equation, the antenna gain estimate, and the array factor in [12]. Although this model only accounts for thermal-noise limited performance, it shows the potential for this technology in a through-wall application.

In this model, the two-way wall attenuation was accounted for as a loss factor. Range resolution was estimated for every pixel inside of the radar field-of-view where the single-image SNR was greater than 13.66 dB. Estimated maximum range
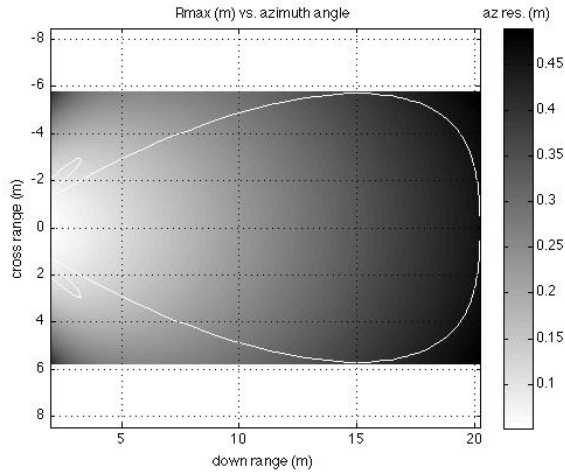
Fig. 8. Estimated maximum range for imaging through a 20.3 cm solid concrete wall, where the white line indicates maximum detection range for a 0 dBsm target with an SNR greater than 13.66 dB.

Fig. 9. A high-clutter free-space target scene.

for a human target (0 dBsm) through a 20.3 cm-thick solid concrete wall with a two-way loss of 90 dB [13] is 20 m with a down-range resolution of 7.5 cm and worst-case cross-range resolution of 45 cm (Fig. 8). At ranges less than 20 m, cross-range resolution is better than 45 cm.

VI. Measured Results

Results are shown as a series of radar images which were collected at an imaging rate of 10.8 Hz. These results show a rapidly moving target without image blurring, high-fidelity images of low-RCS moving targets, and a moving human target through a 10 cm-thick solid concrete wall.

A. Human Rotating a Metal Rod

To show that this radar is capable of imaging in a high-clutter environment with rapid target movements, a human target rotating a metal rod was imaged in a high clutter target scene (Fig. 9).

Range gating and frame-to-frame coherent change detection were used to eliminate clutter, where each data set is coherently subtracted from the previous one. Continuous coherent change detection of the target scene clearly shows the range vs. cross-range imagery of a human target and the specular reflection of the rotating metal rod without noticeable blurring (every-other-frame is shown in Fig.10).

B. 2.5 cm Diameter Metal Spheres

Coherent background subtraction was used to image a pair of 2.5 cm diameter metal spheres located approximately 4 m down-range from the array, where one is stationary and the other rolls past (Fig. 11). Multi-path scattering from the spheres is noticeable as one passes close to the other. The RCS of a 2.54 cm diameter sphere at the radar center frequency of 3 GHz is approximately -29 dBsm. The clear radar images of both the moving and stationary spheres demonstrate the sensitivity of this real-time radar sensor.

C. Through-Wall Imagery

A human target was imaged through a 10 cm-thick solid concrete wall (wall shown in Fig. 12). The radar sensor was placed approximately 6 m from the wall, and the human target was approximately 3 m behind the wall walking away from it. The location of the human target is clearly indicated for every frame (1 of every 3 frames shown in Fig. 13), where the signal-to-clutter ratio appears to be in excess of 15 dB and the wall is not noticeable. This imagery shows that the radar sensor is capable of locating a moving human target through a wall at stand-off ranges in real-time.

VII. GPU Real-Time Imaging Preliminary Results

Core SAR processing routines were developed for a GPU. A GPU is a multi-core processing architecture which provides a high-speed parallel processing platform with upwards of 128 processors (or more depending on the GPU used). GPU kernels were designed to interface with the previously described C++ and MEX interface framework. The SAR processing routine was run on an NVidia GTX 8800 Ultra, which was benchmarked to process RMA SAR image frames with 512 x 2048 pixels at a rate of 70 Hz. This test showed that if a 10.8 Hz image rate is maintained then excess overhead processing time is available for advanced algorithms, such as autofocus, target ID, range-range-doppler processing, or dispersion compensation. These advanced algorithms will be essential to fielding a practical system to an end user, where detections and tracks are clearly presented on a radar screen.

VIII. Conclusions

A through-wall radar sensor was shown to be capable of geo-locating a human through a 10 cm-solid concrete wall at stand-off ranges providing video frame-rate imaging at 10.8 Hz. In addition, -29 dBsm spheres were imaged in free-space while one rolled past the other. Furthermore, a human target rotating a large metal pole was imaged in free-space showing that blurring is not a problem for this radar system while
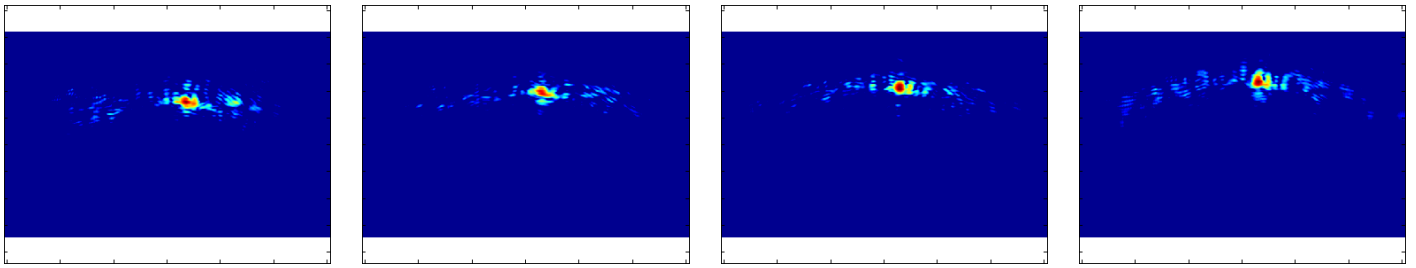
Fig. 13.   Human target through a 10 cm-solid concrete wall (imagery in range vs. cross-range, 20 dB of dynamic range shown).

imaging rapidly moving targets in a high clutter environment. Based on the system model it is expected that this system will locate moving human targets up to 20 m away through a 20 cm-thick solid concrete wall. Future work will include verification of the system model by additional free-space and through-wall testing with the goal of developing of a rapid prototype to be tested in the field.

REFERENCES

[1] S. Nag, M. A. Barnes, T. Payment, and G. W. Holladay, "An ultra-wideband through-wall radar for detecting the motion of people in real time," Radar Sensor Technology and Data Visualization, Proceedings of SPIE Volume 4744, 2002.

[2] D. L. Sostanovsky, A. O. Boryssenko, E. S. Boryssenko, "UWB radar imaging system with two-element receiving array antenna," IEEE 5th International Conference on Antenna Theory and Techniques, pp. 357-360, 24-27 May 2005.

[3] A. Berri and R. Daisy, "High-resolution through-wall imaging," Sensors, and Command, Control, Communications, and Intelligence (C3I) Technologies for Homeland Security and Homeland Defense V, Proceedings of SPIE Volume 6201, 6201J, 2006.

[4] K. Browne, R. J. Burkholder, J. L. Volakis, "Low-cost flat-panel array for through wall opportunistic sensing," 2009 IEEE International Symposium on Antennas & Propagation & USNC/URSI, 1-5 June 2009.

[5] A. Hunt, "Through the wall imaging radar," Air Force Research Laboratory, Rome Research Site, Final Technical Report AFRL-IF-RS-TR-2003-53, March 2003.

[6] A. Martone, R. Innocenti, K. Ranney, "Moving target indication for transparent urban structures," Army Research Laboratory, Technical Report ARL-TR-4809, May 2009.

[7] G. L. Charvat, "A Low-Power Radar Imaging System," Ph.D. dissertation, Deptartment of Electrical and Computer Engineering, Michigan State University, East Lansing, MI, August 2007.

[8] G. L. Charvat, L. C. Kempel, E. J. Rothwell, C. Coleman, and E. L. Mokole, "A through-dielectric radar imaging system," IEEE Transactions on Antennas and Propagation, Accepted January 31, 2010.

[9] G. L. Charvat, L. C. Kempel, E. J. Rothwell, C. Coleman, E. J. Mokole, "An ultrawideband (UWB) switched- antenna-array radar imaging system," Waltham, MA: IEEE International Symposium on Phased Array Systems & Technology,October 2010.

[10] T. S. Ralston, D. L. Marks, P. S. Carney, S. A. Boppart, "Real-time interferometric synthetic aperture microscopy." Optics Express, vol. 16, no. 4, February 2008.

[11] W. G. Carrara, R. S. Goodman, and R. M. Majewski, Spotlight Synthetic Aperture Radar Signal Processing Algorithms, Artech House, Boston, MA, 1995.

[12] G. L. Charvat, T. S. Ralston, J. E. Peabody, "A Through-Wall Real-Time MIMO Radar Sensor for use at Stand-off Ranges," Orlando FL: MSS Tri-Services Radar Symposium, June 2010.

[13] P. R. Hirschler-Marchand, "Penetration losses in construction materials and buildings," MIT Lincoln Laboratory Project Report TrACC-1 Rev. 1, 19 July 2006.
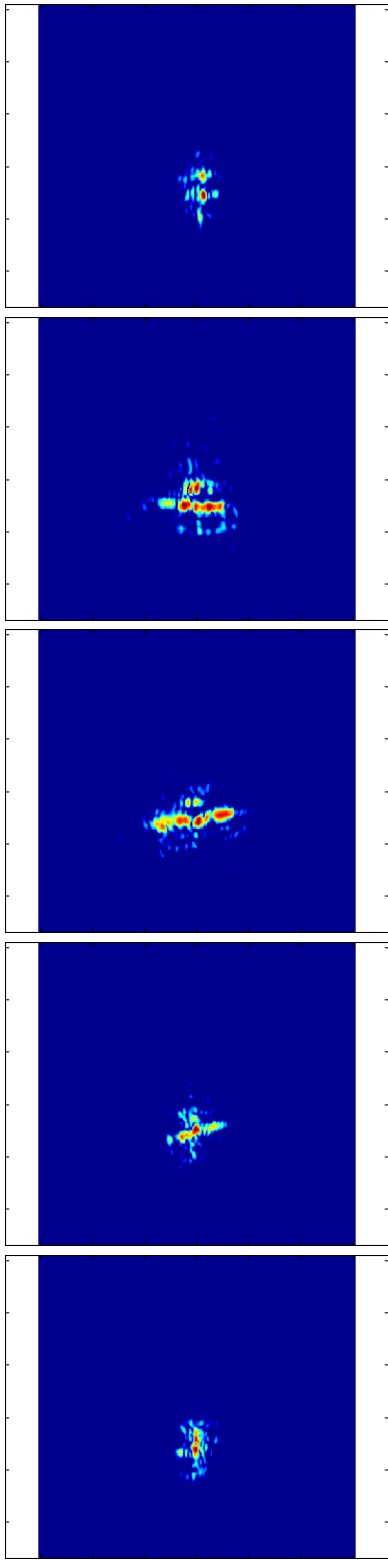
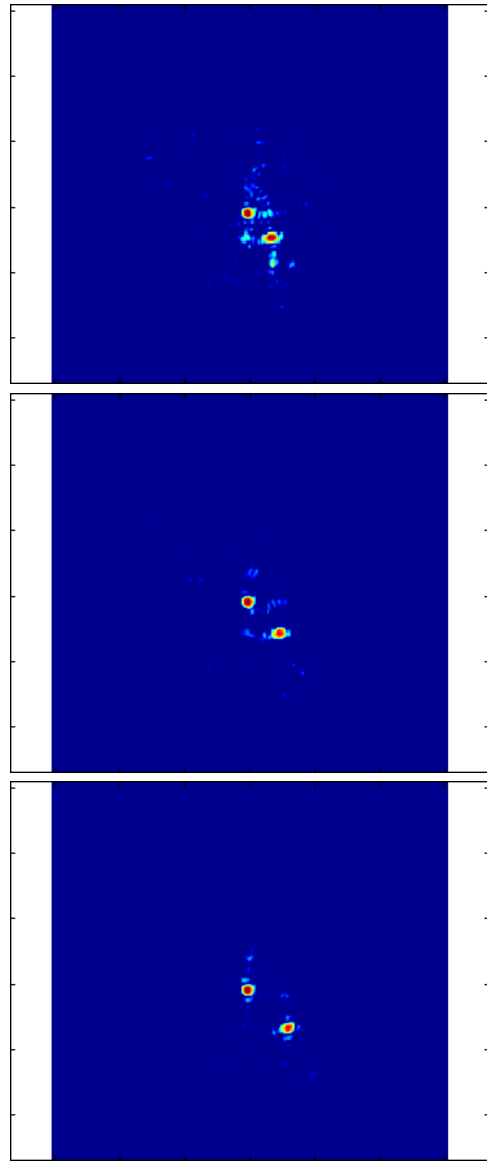Fig. 10. Human rotating a metal rod (imagery in range vs. cross-range, 20 dB of dynamic range shown).

Fig. 11. One 2.5 cm-diameter metal sphere rolls past another in real-time (imagery in range vs. cross-range, 20 dB of dynamic range shown).

Fig. 12. The 10 cm thick solid concrete test wall.